Adapting observationally based metrics of biogeophysical feedbacks from land cover/land use change to climate modeling

2016 Environ. Res. Lett. 11 034002

(http://iopscience.iop.org/1748-9326/11/3/034002)

Environmental Research Letters

LETTER

Adapting observationally based metrics of biogeophysical feedbacks from land cover/land use change to climate modeling

Liang Chen[1] **and Paul A Dirmeyer**

Center for Ocean-Land-Atmosphere Studies, George Mason University, Fairfax, VA, USA

[1] Author to whom any correspondence should be addressed.

E-mail: lchen15@gmu.edu

Keywords: biogeophysical feedbacks, land cover change, metrics, surface temperature, modeling

Supplementary material for this article is available online

OPEN ACCESS

RECEIVED
23 November 2015

REVISED
2 February 2016

ACCEPTED FOR PUBLICATION
9 February 2016

PUBLISHED
24 February 2016

Abstract

To assess the biogeophysical impacts of land cover/land use change (LCLUC) on surface temperature, two observation-based metrics and their applicability in climate modeling were explored in this study. Both metrics were developed based on the surface energy balance, and provided insight into the contribution of different aspects of land surface change (such as albedo, surface roughness, net radiation and surface heat fluxes) to changing climate. A revision of the first metric, the intrinsic biophysical mechanism, can be used to distinguish the direct and indirect effects of LCLUC on surface temperature. The other, a decomposed temperature metric, gives a straightforward depiction of separate contributions of all components of the surface energy balance. These two metrics well capture observed and model simulated surface temperature changes in response to LCLUC. Results from paired FLUXNET sites and land surface model sensitivity experiments indicate that surface roughness effects usually dominate the direct biogeophysical feedback of LCLUC, while other effects play a secondary role. However, coupled climate model experiments show that these direct effects can be attenuated by large scale atmospheric changes (indirect feedbacks). When applied to real-time transient LCLUC experiments, the metrics also demonstrate usefulness for assessing the performance of climate models and quantifying land–atmosphere interactions in response to LCLUC.

1. Introduction

Many modeling and observational studies have examined feedbacks between land and atmosphere manifest in the energy and water cycles [1–5]. Recent studies have shown land cover/land use change (LCLUC) can alter surface climate through biogeophysical feedbacks, which include the modification of energy, moisture and momentum exchanges between the land and atmosphere [6–9]. If sufficiently large areas are involved in LCLUC, the feedback to the atmosphere can extend from regional to global scales [10]. For a better understanding of climatic variability and future climate projections, current Earth system modeling efforts now consider LCLUC as one of the categories of anthropogenic forcing [11]. However, few studies have explored the plausibility of simulated biogeophysical feedbacks within climate because of the lack of extensive observations or the development of meaningful biogeophysical metrics [12].

The development of flux tower networks that measure the land–atmosphere exchange of energy, moisture, and carbon provides a good platform to quantify and address the uncertainties in land surface models [13]. Some flux towers have been deployed in a manner that makes it possible to quantify the observed biogeophysical feedback of LCLUC. By using neighboring flux tower sites with different land cover conditions, several studies have documented the influence of LCLUC on surface climate, especially on surface temperature [14–21]. Among these studies, Lee *et al* [14] developed a method to examine the 'intrinsic biophysical mechanism' (hereafter IBPM) that separates the biogeophysical effects into three components associated with radiative forcing, surface roughness and the Bowen ratio. Also based on the surface energy

balance, a more thorough decomposed temperature metric (DTM) was proposed by Luyssaert *et al* [15] to analyze the change in surface temperature due to changes in incoming radiation, surface albedo, ground heat, sensible and latent heat fluxes. These approaches were developed with observed data, but they can provide meaningful metrics to assess biogeophysical feedbacks of LCLUC in climate models.

Most current model-based studies simply identify the climatic feedback from LCLUC by calculating the difference between runs that prescribe two contrasting land cover conditions without distinguishing the different feedbacks that arise. Direct feedbacks include alterations of absorbed solar radiation due to albedo changes, and perturbations to the partitioning of net radiation between sensible, latent and ground heat fluxes [8]. Indirect feedbacks are also important [22, 23]. For instance, changes in air temperature may influence circulations or the distribution of snow cover, which in turn affects surface temperature through albedo feedbacks; the effect on humidity may alter cloud distributions that influence incoming radiation at the land surface. Most current observation-based studies have focused on the direct feedback [14, 16, 17]. However, metrics like IBPM and DTM may help us disentangle the direct and indirect biogeophysical feedbacks of LCLUC.

In this paper, IBPM and DTM are used as the basis to investigate direct and indirect feedbacks in FLUXNET observations [24] and the Community Earth System Model (CESM) to demonstrate their potential for the study of the climatic impacts of LCLUC. Section 2 provides a detailed description of the metrics, the models and data used, and the experimental design. Section 3 presents results from the application of the two metrics. Section 4 includes discussion and conclusions.

2. Methodology

2.1. Metrics

2.1.1. Intrinsic biophysical mechanism

The IBPM [14] is based on the surface energy balance:

$$R_n = S + \mathrm{LW_{in}} - \varepsilon\sigma T_s^4 = H + \mathrm{LE} + G, \quad (1)$$

where R_n is net surface radiation, S is net surface shortwave radiation, $\mathrm{LW_{in}}$ is incoming longwave radiation, ε is surface emissivity, σ is the Stephan–Boltzmann constant, T_s is surface temperature, H is sensible heat flux, LE is latent heat flux, and G is ground heat flux. Sensible heat flux is defined from the gradient relationship:

$$H = \rho C_p \frac{T_s - T_a}{r_a} \quad (2)$$

$$\mathrm{LE} = \frac{H}{\beta} \quad (3)$$

expresses latent heat flux in terms of sensible heat flux; ρ is air density, C_p is specific heat of air at constant pressure, T_a is air temperature, r_a is aerodynamic resistance and β is the Bowen ratio. Surface outgoing longwave radiation in (1) can be approximated using a Taylor series expansion with T_a:

$$T_s^4 = T_a^4 + 4T_a^3(T_s - T_a). \quad (4)$$

Using (2) and (3), T_s can be solved from (1):

$$T_s = \frac{\lambda_0}{1+f}(R_n^* - G) + T_a, \quad (5)$$

where R_n^* is apparent net radiation ($R_n^* \approx R_n$) [14], λ_0 is defined as temperature sensitivity [$\lambda_0 = 1/(4\sigma T_a{}^3)$], and f is an energy redistribution factor:

$$f = \frac{\rho C_p}{4\sigma T_a^3 r_a}\left(1 + \frac{1}{\beta}\right). \quad (6)$$

IBPM assumes nearby contrasting land types share the same atmospheric background, such as air temperature and incoming radiation. Ignoring changes in surface emissivity and ground heat flux, surface temperature change ΔT_s can be derived by the first derivative of (5):

$$\Delta T_s \approx \frac{\lambda_0}{1+f}\Delta S + \frac{-\lambda_0}{(1+f)^2} R_n \Delta f, \quad (7)$$

where ΔS is the change of net shortwave radiation, and Δf is the change in the energy redistribution factor, attributable to changes in surface roughness (Δf_1) and Bowen ratio (Δf_2):

$$\Delta f_1 = -\frac{\rho C_p}{4\sigma T_a^3}\left(1 + \frac{1}{\beta}\right)\frac{\Delta r_a}{r_a^2}, \quad (8)$$

$$\Delta f_2 = -\frac{\rho C_p}{4\sigma T_a^3 r_a}\frac{\Delta\beta}{\beta^2}. \quad (9)$$

Due to the assumption of identical meteorological forcings, IBPM does not account for atmospheric feedbacks from LCLUC (indirect effects), and is regarded only as a 'local perturbation superimposed on the changing background' [14]. On larger scales, the changes in the atmospheric background state cannot be ignored. Therefore, a revised IBPM is expressed as:

$$\Delta T_s' \approx \underset{\frac{\lambda_0}{1+f}(\Delta R_n - \Delta G)}{1} + \underset{\frac{-\lambda_0}{(1+f)^2}\times(R_n - G)\Delta f_1}{2} + \underset{\frac{-\lambda_0}{(1+f)^2}\times(R_n - G)\Delta f_2}{3} + \underset{\Delta T_a,}{4} \quad (10)$$

where ΔT_a is the change in air temperature. The ground heat flux is not ignored here because of its considerable change when vegetation is removed, especially over the high latitudes (shown later). On the right-hand side of (10), terms 1, 2 and 3 are similar to the original IBPM. Term 4 includes the change of the atmospheric background, which can be considered an indirect effect of LCLUC on climate. The impact of downward radiation changes is now implicitly

Table 1. Information of paired flux towers.

Pair	Period	Name	Latitide	Longitude	Elevation	Land cover	Separation
1	2005–6	DE-Meh	51.2753	10.6555	286	Grassland	26.04 km
		DE-Hai	51.0793	10.4520	430	Deciduous broadleaf	
2	2007–10	IT-Mbo	46.0156	11.0467	1550	Grassland	19.37 km
		IT-Lav	45.9553	11.2812	1353	Evergreen needleleaf	
3	2007–10	DE-Gri	50.9495	13.5125	385	Grassland	4.13 km
		DE-Tha	50.9636	13.5669	380	Evergreen needleleaf	
4	2006–10	DE-Kli	50.8929	13.5225	480	Cropland	8.46 km
		DE-Tha	50.9636	13.5669	380	Evergreen needleleaf	
5	2005–9	US-NC1	35.8118	−76.7119	5	Open shrub	4.04 km
		US-NC2	35.8030	−76.6685	5	Evergreen needleleaf	
6	2004–7	US-DK1	35.9712	−79.0934	168	Grassland	0.69 km
		US-Dk2	35.9736	−79.1004	168	Deciduous broadleaf	
7	2003–5	CA-SF3	54.0916	−106.0053	540	Open shrub	19.90 km
		CA-SF2	54.2539	−105.8775	520	Evergreen needleleaf	
8	2006–10	US-Fwf	35.4454	−111.7718	2270	Grassland	33.84 km
		US-Fmf	35.1426	−111.7273	2160	Evergreen needleleaf	

included in term 1, which indicates the intrinsic surface sensitivity to the radiative fluxes, which we discuss later. The rest of its impact is reflected in air temperature change.

2.1.2. Decomposition of surface temperature changes

Full decomposition of radiative surface temperature change induced from LCLUC was proposed by Juang *et al* [16] and has been elaborated by Luyssaert *et al* [15]. This method (DTM) is also based on the surface energy and starts with the first derivative of equation (1)

$$\Delta T_s = \frac{1}{4\varepsilon\sigma T_s^3}[-SW_{in}\Delta\alpha_s + (1-\alpha_s)\Delta SW_{in} + \Delta \mathrm{LW}_{in} - \Delta \mathrm{LE} - \Delta H - \Delta G - \delta T_s^4 \delta\varepsilon_s]. \quad (11)$$

To keep consistency with IBPM, surface emissivity changes are also ignored in (11). Therefore, DTM temperature change is:

$$\Delta T_s = \frac{1}{4\sigma T_s^3}[-SW_{in}\Delta\alpha_s + (1-\alpha_s)\Delta SW_{in} + \Delta LW_{in} - \Delta \mathrm{LE} - \Delta H - \Delta G]. \quad (12)$$

Equations (10) and (12) provide two metrics for estimating the change in surface temperature due to land use change from *in situ* measurements or climate model output.

2.2. Observational data

We use observational data from selected paired flux towers obtained from the AmeriFlux network [24] and the European Fluxes Database [25]. Paired sites contain one flux tower located in forest and one in nearby open land (grassland, cropland or open shrub). Such paired sites can represent local land cover change (deforestation in these cases), and their climatic differences can be considered representative of the impact of LCLUC. The selection of paired sites follow two criteria: (1) the data period should be at least one common year between the two sites; (2) the paired sites should have measurements of all necessary variables used to calculate the metrics. Eight pairs of flux towers meet the criteria (table 1), and their locations are shown in figure S1. The average linear distance between the paired sites is 14.5 km, which is less than that in previous paired-site studies [14, 15]. The average meridional difference is 11.4 km, and the average elevation difference is 72 m.

Three-hour daytime and nighttime means are calculated from 30 min level-2 data. Many records would have to be omitted if calculating daily means because of missing data. Observations from 12:00 to 15:00 local standard time (LST) are used for the daytime mean, and 00:00 to 03:00 LST for the nighttime mean.

As reported by Wilson *et al* [26], a mean energy imbalance on the order of 20% is prevalent among FLUXNET sites. Energy imbalances exist at all these paired sites. Figure 1 shows a comparison between daytime net radiation and the sum of latent, sensible and ground heat fluxes at the 16 sites. To ameliorate imbalances, the residual is distributed to the sensible and latent heat fluxes in proportion to the Bowen ratio [27].

2.3. Model sensitivity simulations

The CESM version 1.2.2 is used in this study. CESM is a coupled Earth system model composed of separate climate system components for atmosphere, ocean, land, sea-ice and land-ice [28]. This study is focused on land–atmosphere interactions, so ocean, sea-ice and land-ice components have been deactivated. The Community Atmosphere Model version 5.3 (CAM5.3) [29] and Community Land Model version 4.5 (CLM4.5) [30] simulate the Earth's atmosphere and land respectively.

A set of offline (land-only) and coupled land-cover-change sensitivity experiments have been

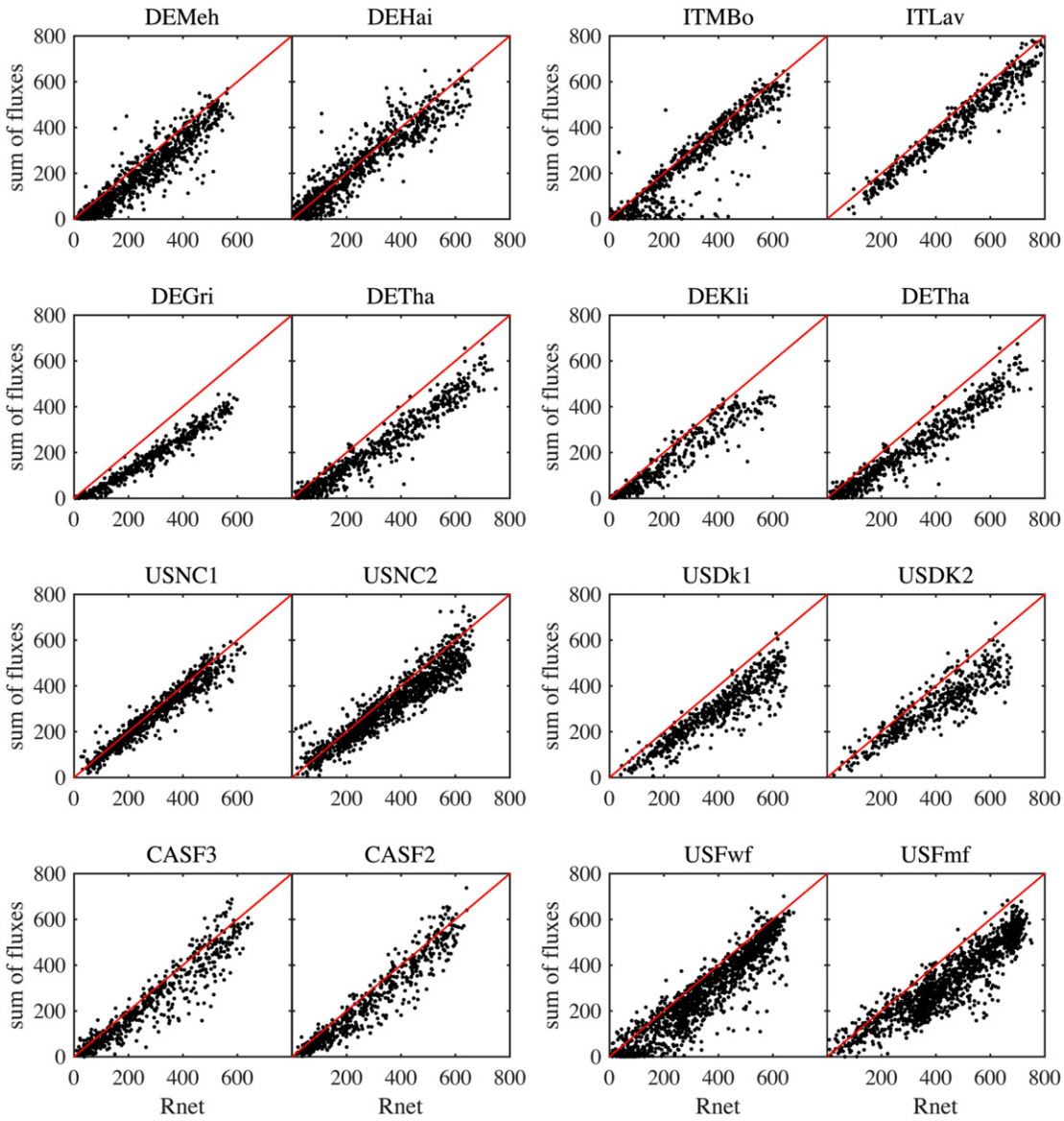

Figure 1. The energy imbalances at paired flux tower sites. Horizontal axis is the net radiation (W m^{-2}); vertical axis is the sum of sensible, latent and ground heat fluxes (W m^{-2}).

Table 2. Land-cover-change experiments in CESM.

	Name	Atmosphere	Land cover
Offline	*Ctrl_off*	Qian	PFTs in 1850
	AllGrass_off	Qian	Replace all non-grass with grass
Coupled	*Ctrl_cpl*	CAM 5.3	PFTs in 1850
	AllGrass_cpl	CAM 5.3	Replace all non-grass with grass

conducted (table 2). As mentioned before, the original IBPM was developed assuming atmospheric feedback is absent. Therefore, 'offline' simulations well represent direct effects of LCLUC, because the atmospheric forcings are the prescribed identically among different land-cover-change experiments. In offline experiments (*Crl_off* and *AllGrass_off*), CLM is driven by global atmospheric forcing data [31]. In coupled experiments (*Ctrl_cpl* and *AllGrass_cpl*), identical prescribed sea surface temperature (SST) and sea ice cover climatologies are used for each simulation with a fixed CO_2 concentration of 284.7 ppm. The prescribed SSTs are a pre-industrial climatology from 1870 to 1890 calculated from a merged product based on the monthly mean Hadley Centre sea ice and SST dataset version 1 (HadISST1) and version 2 of the National Oceanic and Atmospheric Administration weekly optimum interpolation SST analysis [32]. Two land cover scenarios are used: control runs (hereafter referred as *Crl_off* and *Ctrl_cpl* for the offline run and coupled run, respectively) have prescribed land cover conditions from 1850 [33], while 'All Grass' runs (*AllGrass_off* and *AllGrass_cpl*) use a modified global land cover condition where plant functional types (PFTs) which are not grass (non-grass) are replaced with grass. Non-

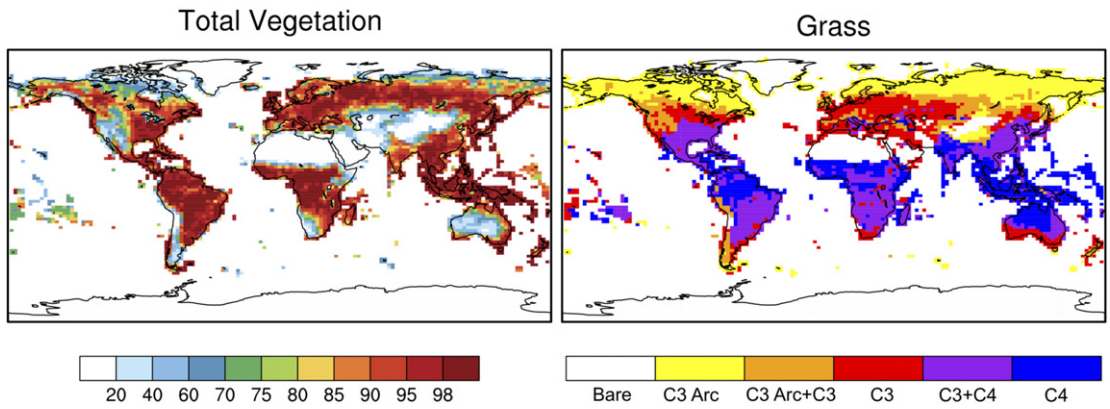

Figure 2. The PFTs distribution in CESM experiments. (a) The percent coverage of all vegetation PFTs; (b) the distribution of three types of grass in the *AllGrass* experiment ('Bare' is bare soil; 'C3 Arc + C3' indicates the coexistence of Arctic C3 and non-Arctic C3 grass in this region; and 'C3 + C4' indicates the coexistence of non-Arctic C3 grass and C4 grass).

grass PFTs located equatorward of 30°N/S are changed to C4 grass, those between 30°N–60°N (or 30°S–60°S) are changed to C3 grass, and those poleward of 60°N/S are changed to arctic C3 grass (figure 2). The total vegetation coverage in each grid box is unchanged; only the distribution of PFTs within each grid box is changed. All simulations are run at a horizontal resolution of 1.9° × 2.5°. We have found that relatively short climate simulations produce a climatological signal of land-cover-induced changes that are nearly indistinguishable from long simulations. In this study, the focus is on development and application of metrics, so 25 year simulations (with 5 years of spin-up) are conducted for each experiment in table 2. We focus primarily on boreal summer (JJA) in this study.

2.4. Transient model simulations

In addition to the land-cover-change sensitivity experiments, CESM output from the Last Millennium Ensemble Project (LME) [34] are also examined. LME provides an ensemble of simulations from both land-cover-change-only and all-forcing (including greenhouse gas, aerosol, ozone and solar variations) experiments for the period 850–2005. The land-cover-change-only experiment considers transient LCLUC but all other forcings remain at their control prescription (see https://www2.cesm.ucar.edu/models/experiments/LME). Details of the transient LCLUC from 1850 to 2005 can be found in [35]. To ensure our results are not biased by the selection of ensemble member, we use all three members from the land-change-only experiment, and three of ten members (numbers 2, 3 and 4) from the all-forcing experiment (member #1 has a different surface data set). Changes in surface temperature are calculated based on ensemble-averaged differences between 1850–1879 (1850s or pre-industrial) and 1976–2005 (2000s or present).

3. Results and discussion

3.1. Validation of metrics in flux tower observations

Figure 3 shows observed and calculated daytime and nighttime surface temperature change from forest to open land, and components from IBPM at paired tower sites. LCLUC leads to an observed daytime warming (+2.23 ± 0.94 K) and a cooling effect at night (−2.05 ± 1.02 K). DTM shows very good agreement with observations, because all components are directly obtained from measurements and energy imbalances have been accounted for. IBPM underestimates the overall warming/cooling effect. The assumption that both land cover types share the same meteorological background is rarely true in actual observations. For example, US-Dk1 and US-Dk2 sites are in adjacent ecosystems [16] and have the smallest separation among the pairs (0.69 km). Figures 4(a)–(c) compare incoming radiation and air temperature between the paired sites with linear regressions, p-values, and biases quantified. The atmospheric background is very similar but not identical between the sites. Differences are most notable for incoming longwave radiative. Figures 4(d)–(f) compare US-Fwf and US-Fmf, which have the largest separation (33.84 km). There is a larger discrepancy there in the atmospheric background, especially for incoming shortwave radiation.

Returning to figure 3, the revised IBPM shows better agreement with observations, especially during night. For the different IBPM components, roughness change exhibits the largest impact (1.96 ± 0.60 K during the day, −1.62 ± 0.61 K at night). Grasslands or croplands are aerodynamically smoother than forest and transfer heat less effectively, thus experiencing higher surface temperatures during daytime and lower surface temperatures at night. The radiation term has a slight cooling effect during day (−0.08 ± 0.07 K), attributable to albedo change cooling being nearly

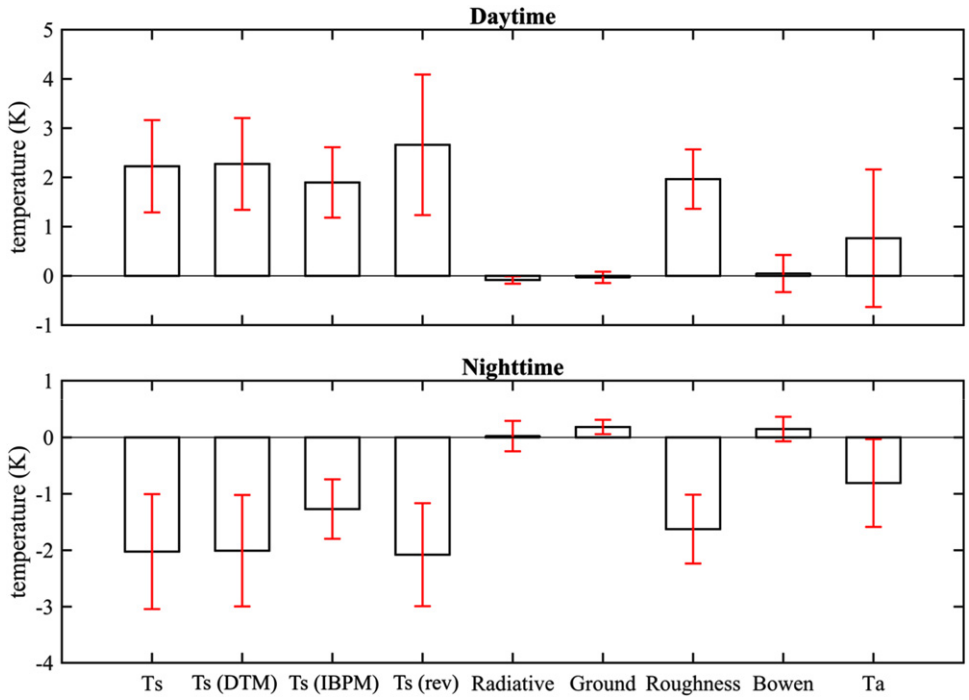

Figure 3. Daytime and nighttime surface temperature change and its components for paired FLUXNET sites, in which 'T_s' is observed surface temperature change, 'T_s (DTM)' is calculated surface temperature change from DTM, 'T_s (IBPM)' is calculated surface temperature change based on the original IBPM, 'T_s (rev)' is surface temperature change calculated based on the revised IBPM, 'Radiative' is intrinsic effect from radiative forcing change, 'Ground' is intrinsic effect from ground heat storage change, 'Roughness' is intrinsic effect associated with roughness change, 'Bowen' is intrinsic effect associated with Bowen ratio change, and 'T_a' is atmospheric (or external) feedback. Red lines indicate the standard deviations among all pairs.

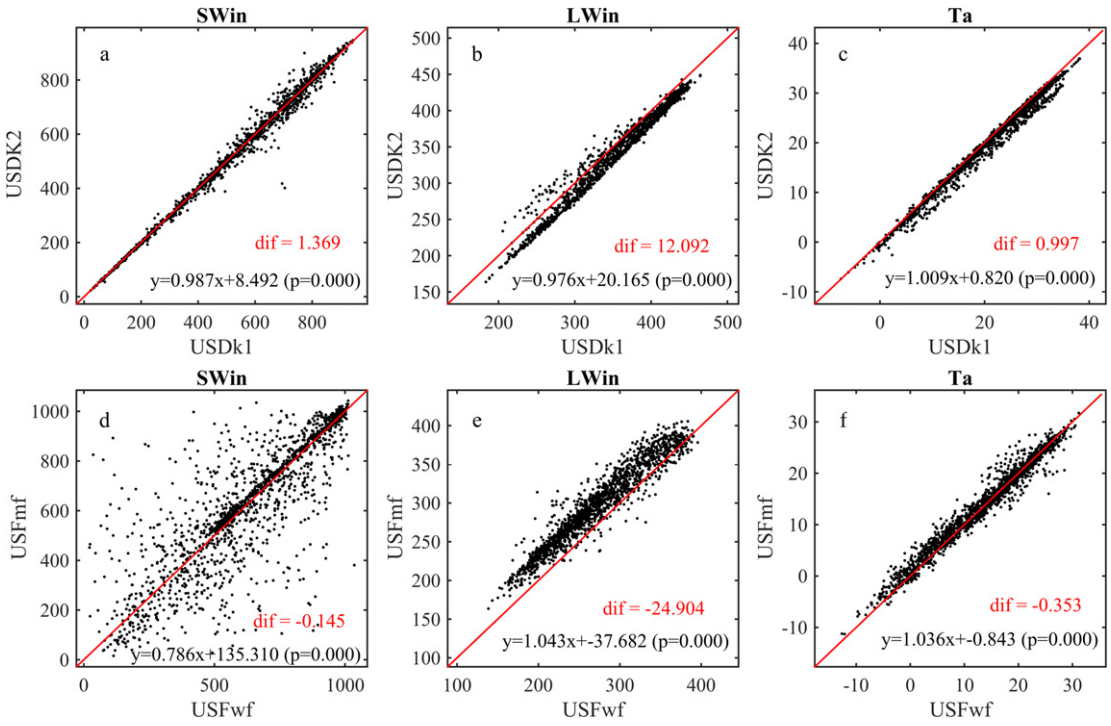

Figure 4. Comparison of incoming shortwave and longwave radiation (W m^{-2}) and surface air temperature (K) between paired sites. The top panel is for USDk1 and USDK2; and the bottom panel is for USFwf and USFmf. The 'dif' shows the average difference (X minus Y) between the paired sites.

offset by more infrared radiation from the warmer surface. Ground heat flux shows a warming effect during nighttime (0.18 ± 0.12 K). The Bowen ratio term is also small compared to roughness.

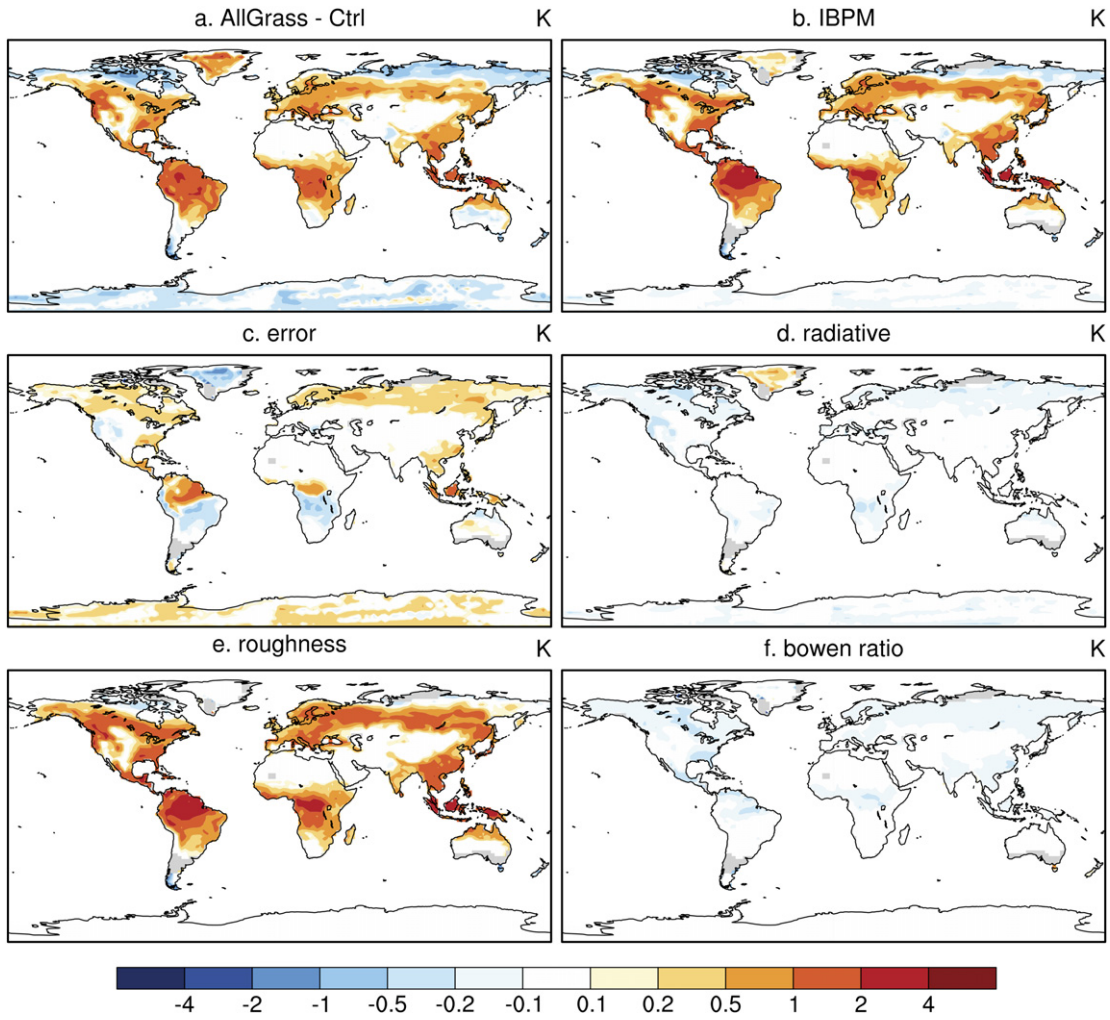

Figure 5. Surface temperature change during JJA from *AllGrass_off—Ctrl_off* experiments. (a) Difference in surface temperature directly calculated from model output; (b) surface temperature change based on IBPM, which consists of radiative forcing associated with albedo change (d), energy redistribution associated with surface roughness change (e) and energy redistribution associated with Bowen ratio change (f), respectively; (c) the error of the IBPM compared to model surface temperature change.

Overall, the metrics show their ability to estimate the surface temperature change based on observational data. However, caution must be observed in this analysis. First, the development of IBPM contains a linearization of surface outgoing longwave radiation (equation (4)), which neglects nonlinear interactions [36]. Second, several terms in equation (10) cannot be directly obtained from observations, and their estimations involve uncertainties. For instance, aerodynamic resistance (r_a) is calculated using equation (2) [36, 37]. Redistribution of the energy balance residual may substantially change sensible heat flux and thus r_a. Also, some observations yield negative resistance values, which are physically meaningless, when measured ($T_s - T_a$) has the opposite sign as measured sensible heat flux. These records have been excluded in the calculations. Due to the uncertainties in estimating r_a, the roughness-related T_s change (term 3) can be up to $\pm$20 K. A threshold is necessary, but in certain conditions observations cannot provide a reliable reference to determine the resistance threshold. We have chosen a threshold of $\pm$5.12 K for term 3 based on its maximum value from the CESM sensitivity experiments. The model-based threshold is chosen for two reasons: (1) energy is conserved every time step; (2) the *AllGrass_off* experiment represents a similar land cover change to the paired sites.

3.2. IBPM in CESM experiments

For offline land-cover-change experiments that satisfy the hypothesis in Lee *et al* [14], the original IBPM (equation (7)) is used to calculate surface temperature change in JJA (figure 5). Generally, the global replacement of forest with grassland increases temperature. The model's averaged global temperature increase is 0.36 K. Cooling effects are only found over higher latitudes where boreal forests were removed. The original IBPM well captures the spatial variability of the model's actual surface temperature change, but there is a slight overestimation of the warming effects. The IBPM-estimated temperature change is 0.45 K at the global scale. The biogeophysical feedback is

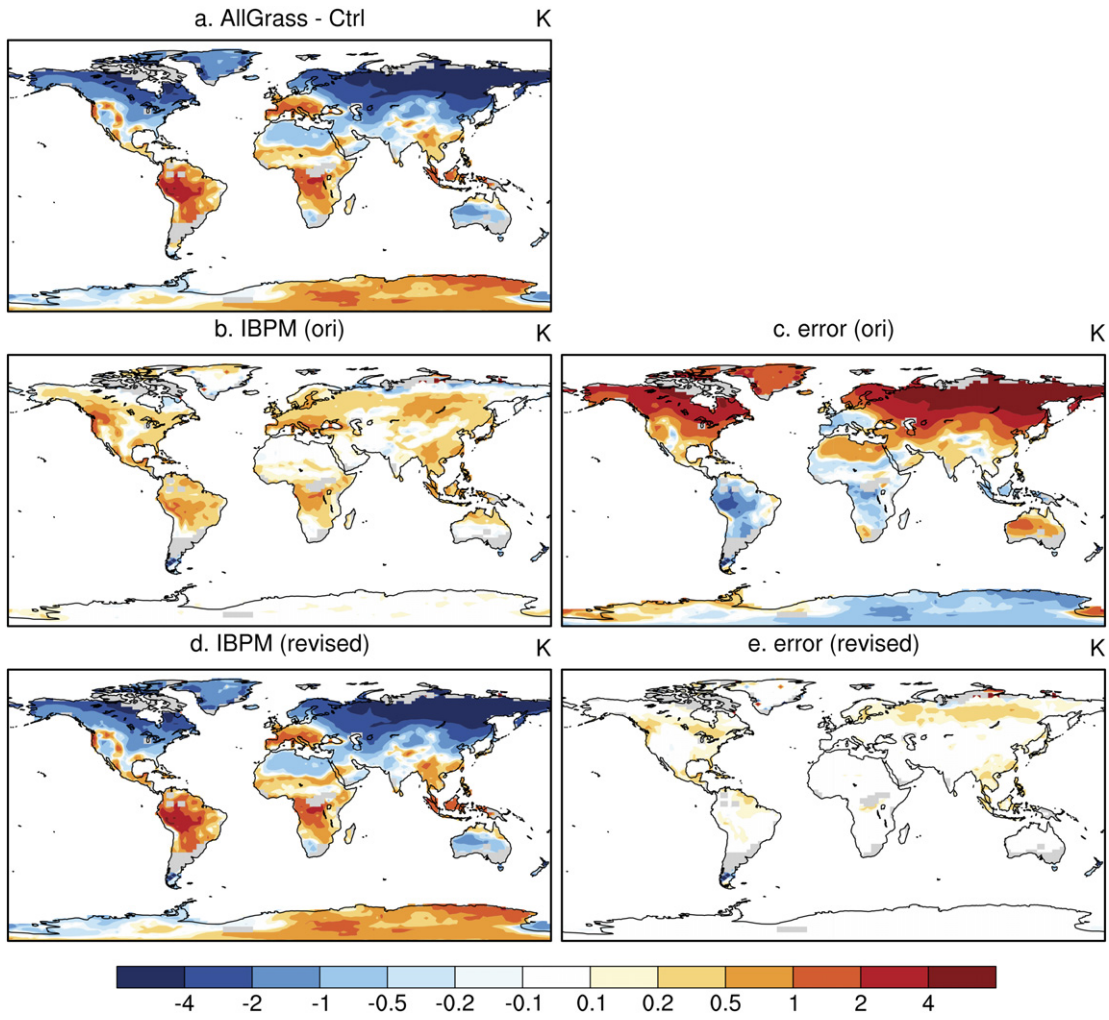

Figure 6. Surface temperature change during JJA from *AllGrass_cpl—Ctrl_cpl* experiments. (a) Difference in surface temperature directly calculated from model output; (b) surface temperature change based on the original IBPM; (c) error of the original IBPM compared to the actual temperature change; (d) surface temperature change based on the revised IBPM; and (e) error of the revised IBPM compared to the model temperature change.

dominated in CLM by surface roughness changes (0.58 K). There is very little temperature change associated with radiative forcing (−0.06 K) or Bowen ratio (−0.07 K), demonstrating consistency with the paired site results. Recall *Ctrl_off* and *AllGrass_off* runs have the same incoming longwave and shortwave radiation. Therefore, the radiative change is attributable only to surface albedo change [14], which is +0.020 in JJA globally averaged over land, and leads to a decrease of 4.06 W m^{-2} in net shortwave radiation. Albedo in DJF has a larger increase (+0.061) due to the effect of exposed snow. The radiative cooling effect in high latitudes is −0.11 K in DJF (figure S2). Bowen ratio changes are determined by both sensible and latent heat flux changes. We found decreased sensible heat flux (globally −8.07 W m^{-2}) attributable largely to decreased surface roughness, but only a slight change in latent heat flux (+1.39 W m^{-2}) (figure S3). Evapotranspiration (ET) and its components in JJA have been examined (not shown). We find increased ET over tropics and boreal forest is due to increased ground evaporation and canopy transpiration, which overcomes the decreased canopy evaporation from lower leaf area index (LAI). ET decreases slightly after deforestation in mid-latitudes. The small change in ET explains the minor contribution of the Bowen ratio term in the original IBPM.

Impacts of LCLUC should not manifest only as local perturbations, but could alter the atmosphere at broader scales. Figure 6 shows the change in surface temperature in the coupled model simulations. When atmospheric feedback is included, deforestation decreases surface temperature in mid- and high latitudes, but increases temperature in the tropics. The global average change is −0.57 K. The original IBPM shows overall warming with the same spatial pattern as the offline run but reduced magnitude to 0.17 K, indicating local perturbations have been attenuated by large-scale atmospheric changes. The revised IBPM shows good agreement with the model's temperature difference (global average of −0.58 K). Therefore, we can separate the direct and indirect impacts of LCLUC

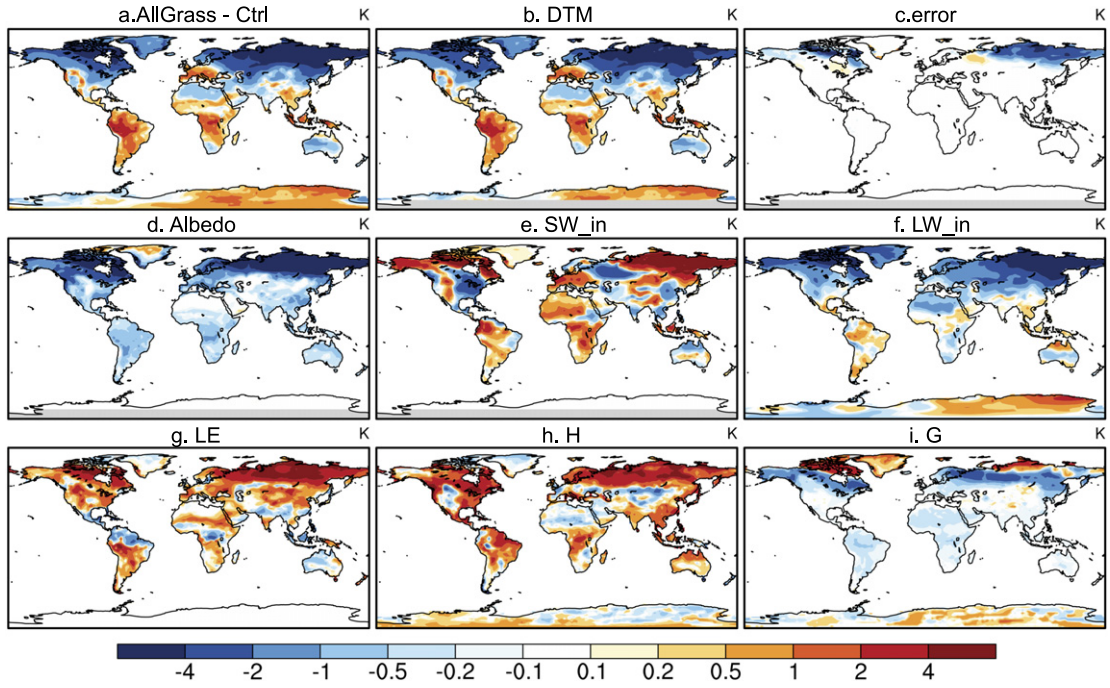

Figure 7. Decomposition of surface temperature change during JJA from *AllGrass_cpl—Ctrl_cpl* experiments. (a) Difference in surface temperature directly calculated from model output (same as figure 6(a)) (b) surface temperature change based on the DTM; (c) bias of decomposed temperature compared to actual surface temperature change; (d)–(i) decomposed surface temperature changes that are individually associated with changes in surface albedo, incoming shortwave radiation, incoming longwave radiation, latent heat flux, sensible heat flux, and ground heat flux.

on climate: direct impacts are represented by the original IBPM, while the atmospheric feedbacks (indirect impacts) are embodied predominantly by the added term ΔT_a (equation (10)).

3.3. DTM in CESM experiments

DTM has also been applied to the coupled experiments (figure 7). DTM-estimated temperature change shows good agreement with model surface temperature change except for a cold bias over the Arctic. Compared with IBPM, DTM provides a detailed breakdown of all components in the surface energy budget. Albedo change causes cooling, especially over Northern Hemisphere high latitudes. Due to the cooling, snow cover is prolonged into summer (now shown) acting as a positive feedback. Effects from incoming shortwave radiation do not show a uniform pattern, but there is consistent warming over many arid regions. Changes in longwave radiation have a cooling effect in most areas of the Northern Hemisphere. Overall, both LE and *H* decrease with land cover change (expect some regions in tropics for LE and some arid areas of middle latitudes for *H*), indicating a general warming effect (note that the sign for the LE and *H* term in equation (12) is negative). The decrease in LE can be associated with lower LAI, decreased temperature and decreased precipitation, and the decrease in *H* can be attributed to surface roughness decreases [21]. The increased LE in some tropical regions (such as the north edge of the Amazon) might be inconsistent with previous studies [38], which found reduced ET when tropical forest is converted to pasture. Such a discrepancy should be attributed to the potential problems with CLM hydrology in simulating ET [39, 40]. The ground heat component shows cooling mainly at high latitudes, because more energy dedicated to snowmelt.

3.4. Application of metrics to LME

Here we apply the metrics to long-term climate simulations designed for realistic transient land-cover-change experiments. Figure 8 shows JJA surface temperature change from pre-industrial to present conditions when only LCLUC is considered. There is warming over agricultural regions in India, Europe and Brazil, but cooling over North America and northern Eurasia. The global averaged change is −0.05 K. The revised IBPM captures the cooling effect of LCLUC (−0.08 K on global average). The small global change in the original IBPM indicates the direct effect has a weak contribution to global temperature in this model. This agrees with previous studies implying LCLUC has a negligible global signature, even though there are significant local impacts [8, 41, 42]. A diminished IBPM effect is found in LME compared with our thorough global deforestation (from no-grass to grass) experiment; LME has much less change in land cover from 1850 to 2005, during which crops and pasture PFTs expand, and their influence is likewise limited.

Applying the IBPM to the all-forcing LME experiments, the direct effect of LCLUC (figure 9(c)) shows a

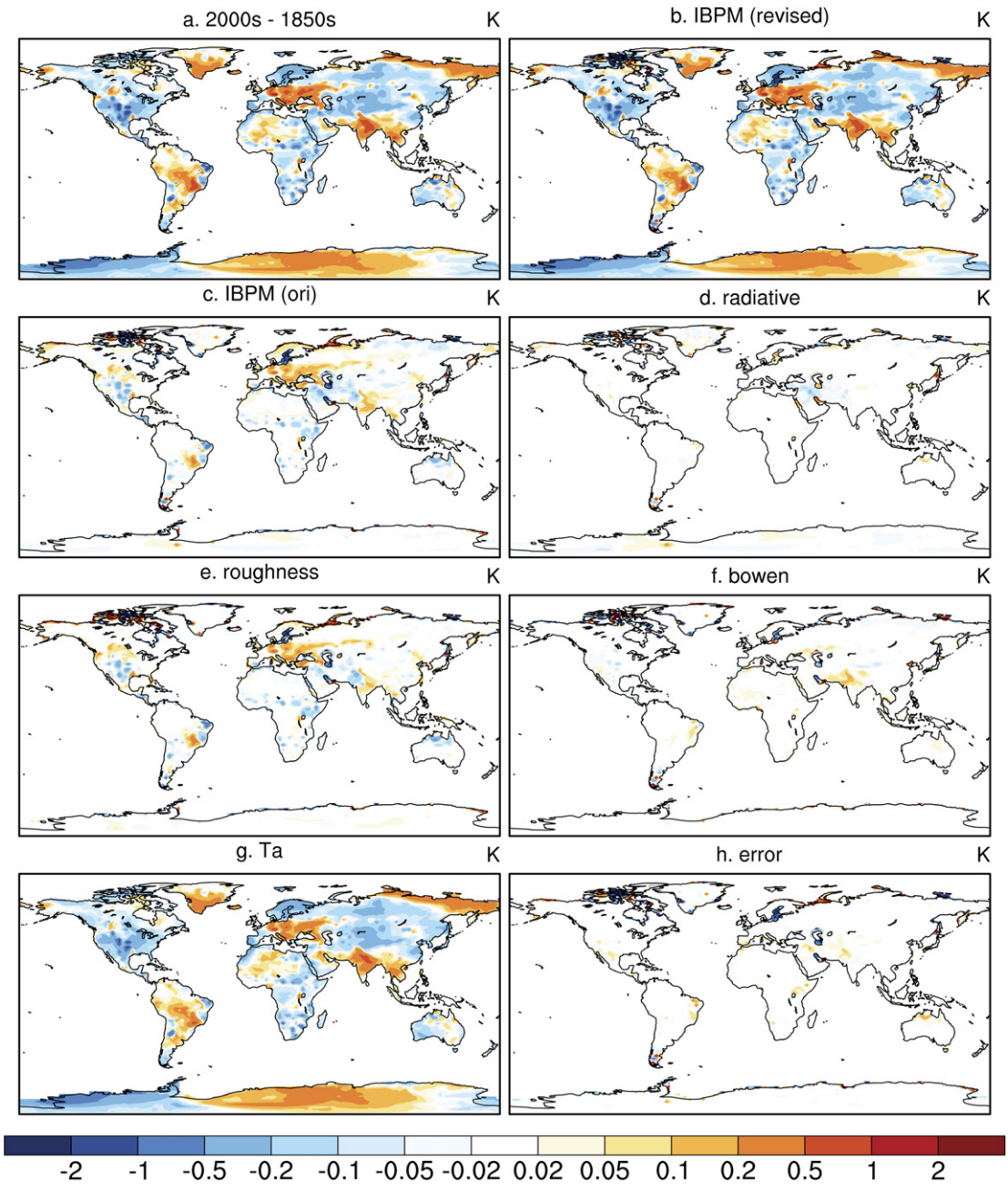

Figure 8. Surface temperature change during JJA from 1850s to 2000s from the land-change-only LME runs. (a) Direct difference in surface temperature; (b) surface temperature change based on the revised IBPM; (c) surface temperature change based on original IBPM; (d)–(g) different components of revised IBPM, which is associated with radiative forcing, surface roughness, Bowen ratio and air temperature; (h) error of revised IBPM compared to model surface temperature change.

similar pattern to that in land-change-only experiments (figure 8(c)), even though the atmospheric background is very different. Radiative- and roughness-related temperature changes are consistent between the experiments, but the Bowen-ratio-related changes account for certain discrepancies. The differences in IBPM are attributable to changes in vegetation phenology as the terrestrial carbon and nitrogen cycles are active in the model. Figure 10 shows the change of leaf area index (LAI) from 1850s to 2000s in land-change-only and all-forcing experiments. LAI decreases in the land-change-only experiment, especially over Eurasia. When all forcings are included, LAI increases over most regions, except parts of East China, Eastern Europe, and Central America. The decrease of LAI in the land-change-only experiment is the result of agricultural expansion and wood harvest, while the increase in the all-forcing experiment implies that other drivers, such as CO_2 fertilization, nitrogen deposition, and longer growing seasons in high latitudes, may exert a larger influence on vegetation growth than anthropogenic LCLUC [35].

DTM shows good agreement with the modeled temperature change for the land-change-only

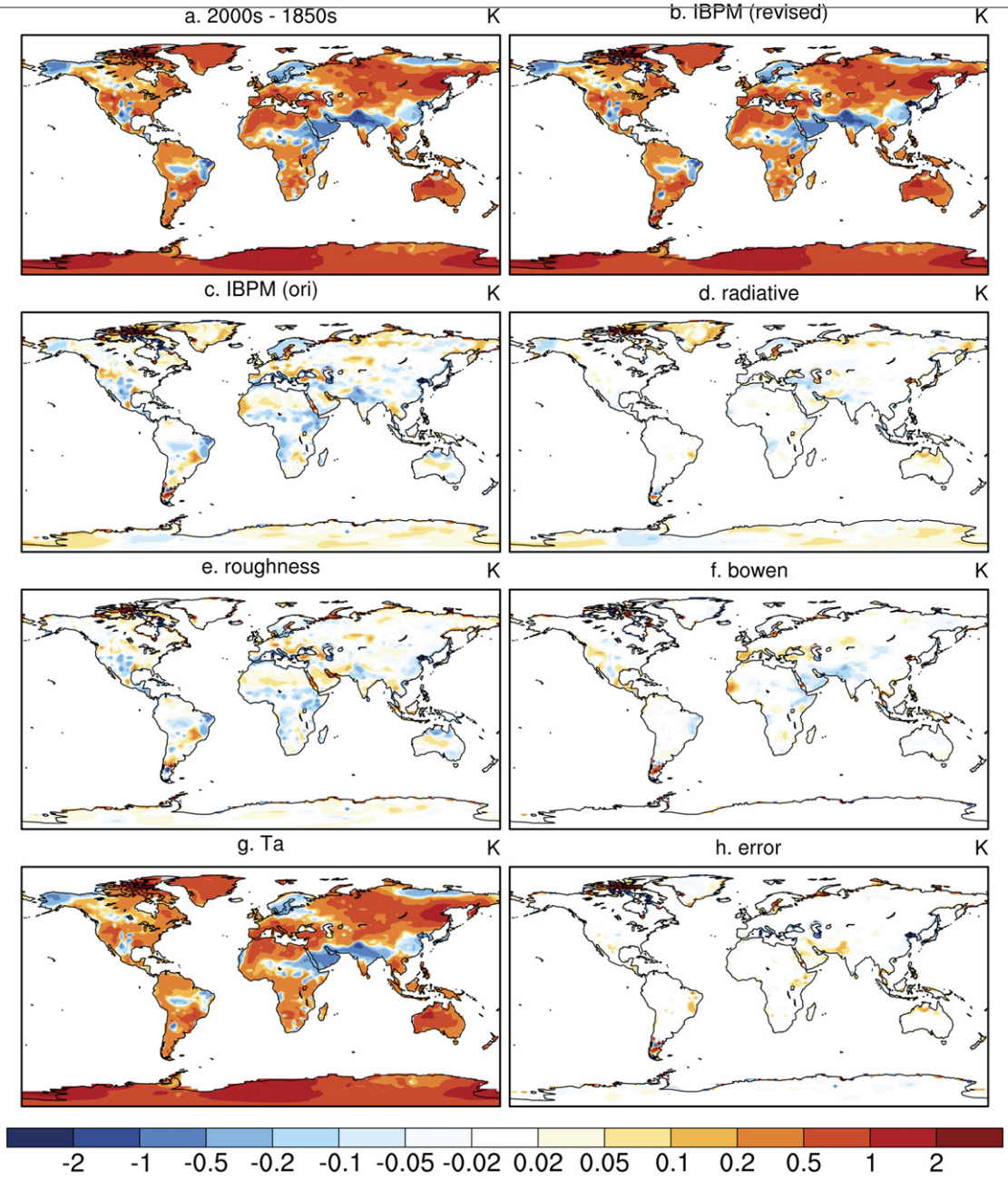

Figure 9. Same as figure 8 but for all-forcings LME runs.

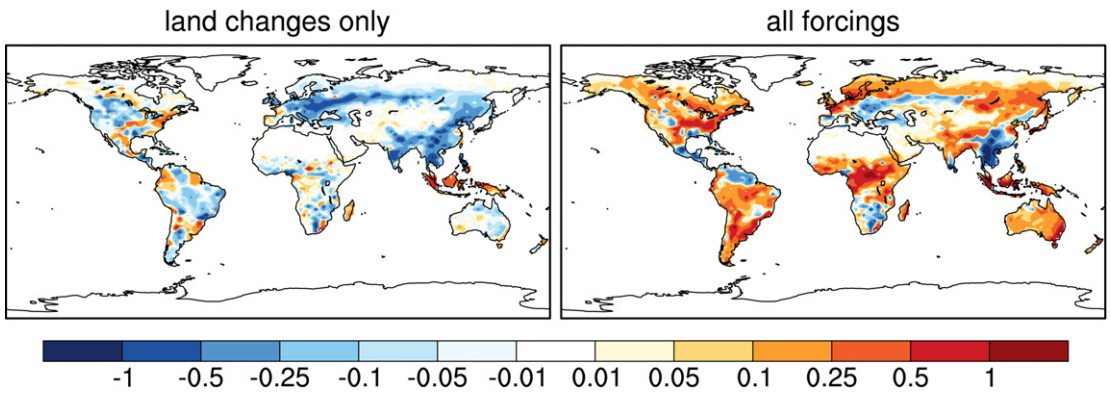

Figure 10. LAI change in JJA from 1850s to 2000s in land-change-only and all-forcings runs.

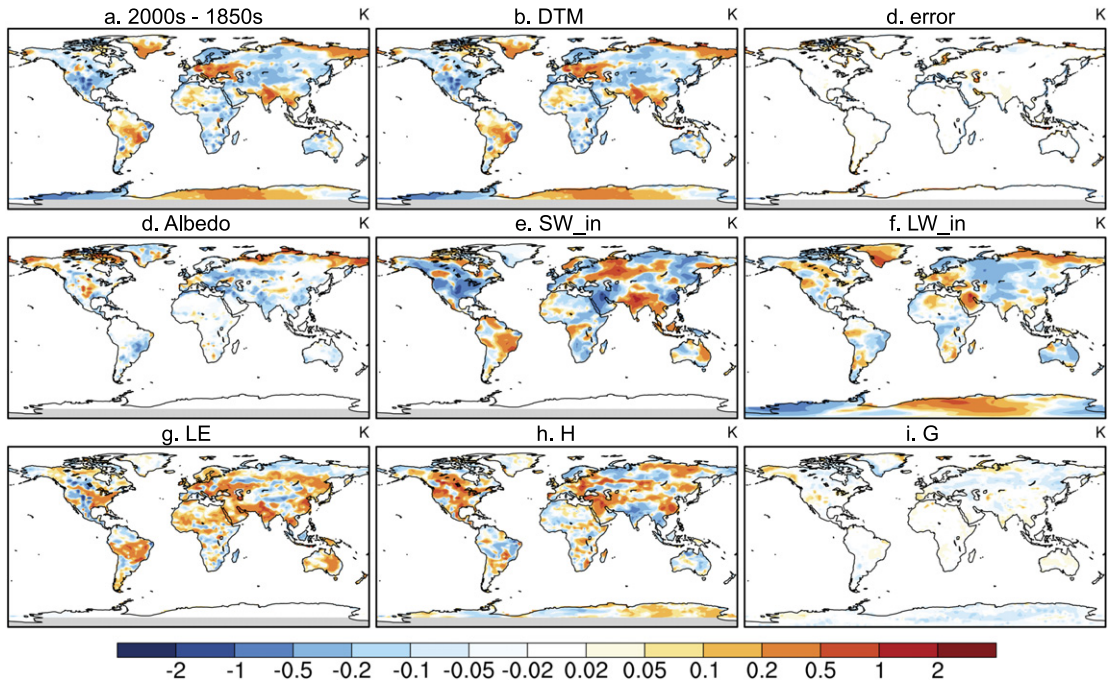

Figure 11. Same as figure 7 but for the surface temperature change from 1850s to 2000s from the land-change-only ensemble runs.

experiment (figure 11). Generally, there is an increase in surface albedo from the 1850s to 2000s, lowering global average surface temperature by about −0.03 K (figure 11(d)). The changes in incoming shortwave and longwave radiation cools global temperature by −0.05 K and −0.03 K, respectively. At low latitudes, these components of incoming radiation often show opposite effects. For instance, greater incoming shortwave radiation is found over central Eurasia and Brazil, where there is decreased incoming longwave radiation; both associated with reduced cloud cover. Latent heat flux decreases due to lower LAI and leads to warming (about 0.04 K globally). Meanwhile, sensible heat flux decreases and warms global surface temperature by another 0.02 K. LCLUC does not have an obvious influence on ground heat flux in this experiment, showing only a small cooling at high latitudes.

4. Conclusions

This paper has explored two observation-based biogeophysical metrics of LCLUC impacts on temperature and their applicability in climate modeling. IBPM and DTM well capture surface temperature changes, and provide insight into the contribution of different surface components (such as albedo, surface roughness, net radiation, and surface heat fluxes) to surface climate.

IBPM [14] is useful to identify the direct impacts of LCLUC on surface temperature. Data from paired FLUXNET sites corroborate offline model sensitivity experiments that show surface roughness effects dominate the biogeophysical feedback of LCLUC at local climate background, while albedo and the Bowen ratio effects play secondary roles. Comparing results from offline and coupled simulations, or land-change-only and all-forcing experiments, there are consistent direct effects, indicating the robustness of IBPM. IBPM requires estimation of unmeasured parameters like aerodynamic resistance and sensitive parameters like Bowen ratio.

Our revision to IBPM shows the ability to represent changes when atmospheric feedbacks (indirect effects) are also considered. Both direct and indirect effects of LCLUC can then be identified. Coupled sensitivity experiments and long-term transient LCLUC experiments suggest that indirect effects can eclipse direct effects on regional to global scales.

DTM [15] shows better agreement with simulated temperature changes in coupled climate models. It provides a straightforward depiction of contributions from all components of the surface energy balance. All the components for this metric can be directly obtained from surface flux observations (where complete) or model output without derived parameters.

Development of metrics like these will help the climate modeling community validate climate model performance in simulating the response to LCLUC. Past model comparison studies [23] struggled to reconcile conflicting temperature and flux responses to land use change among models [41]. Verifiable LCLUC metrics can be used to diagnose the climate sensitivity in Earth system models, especially for the upcoming Land-Use Model Intercomparison Project (LUMIP, https://cmip.ucar.edu/lumip). The two metrics used in this study are focused on the surface energy balance; metrics related to the surface water balance should also be considered to quantify impacts

of LCLUC directly on soil moisture and runoff, and indirectly on precipitation.

Acknowledgments

The authors wish to thank David Lawrence and Ahmed Tawfik at the National Center for Atmospheric Research for their assistance and helpful comments. All the observational data sets used in this study are obtained from the AmeriFlux network (http://ameriflux.ornl.gov/) and the European Fluxes Database Cluster (http://www.europefluxdata.eu/). We thank all site investigators and flux networks for their work to make our metric evaluation possible. LME data provided by the CESM1(CAM5) Last Millennium Ensemble Community Project and supercomputing resources for LME and both offline and coupled land-cover-change sensitivity experiments were provided by the NSF/CISL/Yellowstone supercomputing facility. This study was supported by the National Science Foundation (AGS-1419445). We also are grateful to the anonymous reviewers whose insightful comments helped improve our manuscript.

References

[1] Betts A K, Ball J H, Beljaars A C M, Miller M J and Viterbo P A 1996 The land surface-atmosphere interaction: a review based on observational and global modeling perspectives *J. Geophys. Res.: Atmos.* **101** 7209–25

[2] Findell K L and Eltahir E A B 2003 Atmospheric controls on soil moisture–boundary layer interactions: I. Framework development *J. Hydrometeorol.* **4** 552–69

[3] Koster R D *et al* 2004 Regions of strong coupling between soil moisture and precipitation *Science* **305** 1138–40

[4] Dirmeyer P A 2011 The terrestrial segment of soil moisture–climate coupling *Geophys. Res. Lett.* **38** L16702

[5] Santanello J A, Peters-Lidard C D and Kumar S V 2011 Diagnosing the sensitivity of local land–atmosphere coupling via the soil moisture–boundary layer interaction *J. Hydrometeorol.* **12** 766–86

[6] Oleson K W, Bonan G B, Levis S and Vertenstein M 2004 Effects of land use change on North American climate: impact of surface datasets and model biogeophysics *Clim. Dyn.* **23** 117–32

[7] Bonan G B 2008 Forests and climate change: forcings, feedbacks, and the climate benefits of forests *Science* **320** 1444–9

[8] Pielke R A *et al* 2011 Land use/land cover changes and climate: modeling analysis and observational evidence *Wiley Interdiscip. Rev.: Clim. Change* **2** 828–50

[9] Devaraju N, Bala G and Nemani R 2015 Modelling the influence of land-use changes on biophysical and biochemical interactions at regional and global scales *Plant Cell Environ.* **38** 1931–46

[10] Mahmood R *et al* 2014 Land cover changes and their biogeophysical effects on climate *Int. J. Climatol.* **34** 929–53

[11] Feddema J J *et al* 2005 The importance of land-cover change in simulating future climates *Science* **310** 1674–8

[12] Bright R M, Zhao K, Jackson R B and Cherubini F 2015 Quantifying surface albedo and other direct biogeophysical climate forcings of forestry activities *Glob. Change Biol.* **21** 3246–66

[13] Williams M *et al* 2009 Improving land surface models with FLUXNET data *Biogeosciences* **6** 1341–59

[14] Lee X *et al* 2011 Observed increase in local cooling effect of deforestation at higher latitudes *Nature* **479** 384–7

[15] Luyssaert S *et al* 2014 Land management and land-cover change have impacts of similar magnitude on surface temperature *Nat. Clim. Change* **4** 389–93

[16] Juang J-Y, Katul G, Siqueira M, Stoy P and Novick K 2007 Separating the effects of albedo from eco-physiological changes on surface temperature along a successional chronosequence in the southeastern United States *Geophys. Res. Lett.* **34** L21408

[17] Zhang M *et al* 2014 Response of surface air temperature to small-scale land clearing across latitudes *Environ. Res. Lett.* **9** 034002

[18] Baldocchi D and Ma S 2013 How will land use affect air temperature in the surface boundary layer? Lessons learned from a comparative study on the energy balance of an oak savanna and annual grassland in California, USA *Tellus* B **65** 19994

[19] Betts A K, Desjardins R, Worth D and Cerkowniak D 2013 Impact of land use change on the diurnal cycle climate of the Canadian Prairies *J. Geophys. Res.: Atmos.* **118** 11996–2011

[20] Zhao K and Jackson R B 2013 Biophysical forcings of land-use changes from potential forestry activities in North America *Ecological Monogr.* **84** 329–53

[21] Vanden Broucke S, Luyssaert S, Davin E L, Janssens I and van Lipzig N 2015 New insights in the capability of climate models to simulate the impact of LUC based on temperature decomposition of paired site observations *J. Geophys. Res.: Atmos.* **120** 5417–36

[22] Boisier J P, de Noblet-Ducoudré N and Ciais P 2013 Inferring past land use-induced changes in surface albedo from satellite observations: a useful tool to evaluate model simulations *Biogeosciences* **10** 1501–16

[23] Boisier J P *et al* 2012 Attributing the impacts of land-cover changes in temperate regions on surface temperature and heat fluxes to specific causes: results from the first LUCID set of simulations *J. Geophys. Res.: Atmos.* **117** D12116

[24] Baldocchi D *et al* 2001 FLUXNET: a new tool to study the temporal and spatial variability of ecosystem–scale carbon dioxide, water vapor, and energy flux densities *Bull. Am. Meteorol. Soc.* **82** 2415–34

[25] Aubinet M *et al* 1999 Estimates of the annual net carbon and water exchange of forests: the EUROFLUX methodology *Adv. Ecological Res.* **30** 113–75

[26] Wilson K *et al* 2002 Energy balance closure at FLUXNET sites *Agric. Forest Meteorol.* **113** 223–43

[27] Foken T 2008 The energy balance closure problem: an overview *Ecological Appl.* **18** 1351–67

[28] Vertenstein M *et al* 2013 *CESM User's Guide, CESM1.2 Release Series User's Guide, NCAR Technical Note* (Boulder, CO: National Center for Atmospheric Research) p 884 (http://cesm.ucar.edu/models/cesm1.2/cesm/doc/usersguide/ug.pdf)

[29] Neale R B *et al* 2012 *Description of the NCAR Community Atmosphere Model (CAM5.0), NCAR Technical Note, NCAR/TN-486 + STR* (Boulder, CO: National Center for Atmospheric Research) 274 pp (available at http://cesm.ucar.edu/models/cesm1.0/cam/docs/description/cam5_desc.pdf)

[30] Oleson K W *et al* 2013 *Technical Description of Version 4.5 of the Community Land Model (CLM), NCAR Technical Note, TN-503 + STR* (Boulder, CO: National Center for Atmospheric Research) 434 pp (available at http://cesm.ucar.edu/models/cesm1.2/clm/CLM45_Tech_Note.pdf)

[31] Qian T, Dai A, Trenberth K E and Oleson K W 2006 Simulation of global land surface conditions from 1948 to 2004: I. Forcing data and evaluations *J. Hydrometeorol.* **7** 953–75

[32] Hurrell J W, Hack J J, Shea D, Caron J M and Rosinski J 2008 A new sea surface temperature and sea ice boundary dataset for the community atmosphere model *J. Clim.* **21** 5145–53

[33] Lawrence P J and Chase T N 2010 Investigating the climate impacts of global land cover change in the community climate system model *Int. J. Climatol.* **30** 2066–87
[34] Otto-Bliesner B L *et al* 2015 Climate variability and change since 850 C.E.: an ensemble approach with the community earth system model (CESM) *Bull. Am. Meteorol. Soc.* (doi:10.1175/BAMS-D-14-00233.1)
[35] Lawrence P J *et al* 2012 Simulating the biogeochemical and biogeophysical impacts of transient land cover change and wood harvest in the community climate system model (CCSM4) from 1850 to 2100 *J. Clim.* **25** 3071–95
[36] Zhao L, Lee X, Smith R B and Oleson K 2014 Strong contributions of local background climate to urban heat islands *Nature* **511** 216–9
[37] Liu S, Lu L, Mao D and Jia L 2007 Evaluating parameterizations of aerodynamic resistance to heat transfer using field measurements *Hydrol. Earth Syst. Sci.* **11** 769–83
[38] Lawrence D and Vandecar K 2015 Effects of tropical deforestation on climate and agriculture *Nat. Clim. Change* **5** 27–36
[39] Swenson S C and Lawrence D M 2014 Assessing a dry surface layer-based soil resistance parameterization for the community land model using GRACE and FLUXNET-MTE data *J. Geophys. Res.: Atmos.* **119** 299–210
[40] Tang J *et al* 2015 Incorporating root hydraulic redistribution in CLM4.5: effects on predicted site and global evapotranspiration, soil moisture, and water storage *J. Adv. Model. Earth Syst.* **7** 1828–48
[41] Pitman A J *et al* 2009 Uncertainties in climate responses to past land cover change: first results from the LUCID intercomparison study *Geophys. Res. Lett.* **36** L14814
[42] de Noblet-Ducoudré N *et al* 2012 Determining robust impacts of land-use-induced land cover changes on surface climate over North America and Eurasia: results from the first set of LUCID experiments *J. Clim.* **25** 3261–81